A synthetic strategy for mimicking the extracellular matrix provides new insight about tumor cell migration†

Michael P. Schwartz,[a] Benjamin D. Fairbanks,[a] Robert E. Rogers,[a] Rajagopal Rangarajan,[b] Muhammad H. Zaman[c] and Kristi S. Anseth*[a]

Understanding the role of the tumor microenvironment during cancer progression and metastasis is complicated by interactions between cells, the extracellular matrix (ECM), and a variety of biomolecules. Using a synthetic strategy, we investigated proteolytic modes of migration for HT-1080 fibrosarcoma cells in an environment that limited confounding extracellular influences. A large percentage of HT-1080s migrated through a Rho kinase (ROCK)-dependent rounded morphology with a leading edge protrusion that defined the direction of migration, and migration was only weakly dependent on the adhesive peptide RGDS. HT-1080s migrating in thiol-ene hydrogels are more rounded and exhibit much more invasive behavior than dermal fibroblasts. Our results indicate that HT-1080s have the capacity to migrate through a mechanism that is distinct from mesenchymal cells, with significant amoeboid character even when utilizing a proteolytic migration strategy. The migration mode observed here provides insight into the invasiveness of metastatic cells *in vivo* and demonstrates the potential of a synthetic strategy for investigating complex biological problems.

Introduction

Cancer progression and metastasis are characterized by a complex, reciprocal communication between a tumor and the extracellular environment.[1–4] While much of the basic understanding of cancer biology has been worked out in 2 dimensions,[5] there remains a great need for improved 3-dimensional culture systems that capture the complexity of the natural tumor microenvironment.[6] Not surprisingly, moving to the third dimension alters fundamental aspects of cell migration and tumor growth such as cell polarity, cell morphology, the nature of adhesive contacts, and the necessity for proteolysis to remove physical barriers not encountered in artificial 2-dimensional environments.[7–10]

Further complicating the overall picture and obscuring attempts to develop therapeutic strategies, recent work has demonstrated that cancer cells have the capacity to alter their mode of motility when subjected to external stimuli such as blocking or down-regulating integrin binding or proteolysis.[10–15] In particular, cancer cells will undergo a mesenchymal–amoeboid transition (MAT) or switch from collective to amoeboid migration upon interruption of proteolysis or integrin binding.[10–15] In the specific case of the MAT, elongated, proteolytically dependent cells adopt a rounded proteolytically independent migration strategy when proteolysis is blocked.[12] However, while biomaterials composed of naturally derived ECM components provide a 3-dimensional environment that is seemingly ideal for studying cancer biology, preparation procedures can directly influence cell behavior and results may not be physiologically relevant. For example, the MAT for HT-1080 fibrosarcoma cells was observed in pepsin-extracted collagen[12] but not acid-extracted collagen of similar network structure.[9,16,17] Additionally, cancer cells migrating in

[a] Howard Hughes Medical Institute and Department of Chemical and Biological Engineering, University of Colorado at Boulder, ECCH111, CB424, Boulder, CO 80309. E-mail: kristi.anseth@colorado.edu
[b] Department of Biomedical Engineering, University of Texas at Austin, Austin
[c] Department of Biomedical Engineering, Boston University, Boston

† Electronic supplementary information (ESI) available: Supplemental figures showing integrin dependence and persistence fits; Details for calculation of mesh size; Supplemental movies demonstrating cell division, migration morphologies in 2D and 3D, and formation of constriction rings. See DOI: 10.1039/b912438a.

Insight, innovation, and integration

Here, we demonstrate that an engineering approach leads to new insight about the invasive behavior of cancer cells. Our synthetic approach enables quantitative study of cancer biology through systematic incorporation of specific extra-cellular matrix components while minimizing confounding biological interactions. While we demonstrate the design of a material for studying cancer migration and proliferation, this technology could prove to be generally useful for studying a wide variety of biological phenomena since many types of biomolecules could be incorporated into the synthetic design.

an *in vivo* environment have been observed to be morphologically similar to rounded, rather than elongated, cells *in vitro*.[12,17] Therefore, moving to the third dimension introduces significant complexity, and care must be taken when drawing conclusions from results obtained with culture materials derived from single ECM components.

Due to the overwhelming complexity of how cells interact with even the simplest naturally derived biomaterials, there is growing motivation to take a reductionist approach in designing 3-dimensional culture platforms.[18,19] Previously, researchers have demonstrated that synthetic hydrogels can be designed to mimic critical aspects of ECM function and that cell spreading and migration in these materials closely mimics behavior in natural biomaterials.[20–26] Strategies such as these provide explicit control over how biomolecules are presented to cells, and provide researchers with tools for simplifying the 3-dimensional environment to focus on the role of specific cell–ECM interactions in biological processes such as cell migration. Thus, new strategies for designing synthetic ECM mimics and validating their use will encourage biological researchers to incorporate an engineering approach into their current methods and hopefully lead to new fundamental discoveries.

The goal for this work was to quantify how adhesion influences migration of HT-1080s in a 3-dimensional environment, with an emphasis on probing proteolytically-dependent modes of motility. Taking advantage of principles previously reported for synthesizing biomimetic hydrogels,[20–22,24,25] we developed a 3-dimensional ECM mimic[22] with a mesh size that is much smaller than the size of a cell to limit migration to proteolytic mechanisms, and with a poly(ethylene glycol) backbone to reduce confounding biological interactions. To our surprise, we found that HT-1080s migrated primarily through a Rho kinase (ROCK)-dependent rounded morphology that was only weakly dependent on integrin receptor interactions. We quantitatively determined that the morphology of HT-1080s migrating in thiol-ene hydrogels closely resembles *in vivo* migrating cells and *in vitro* amoeboid cells,[12] but is very different compared with dermal fibroblasts, a model mesenchymal cell type. These results suggest that the physiological mechanism for HT-1080 migration may be very different than the elongated mode previously observed in collagen,[12] and demonstrates a system that may be ideal for studying cancer invasiveness.

Results

Fig. 1 illustrates the polymerization scheme used for this work. Hydrogels were synthesized using a thiol-ene photopolymerization mechanism to copolymerize ene-functionalized poly(ethylene glycol) (PEG) precursors with thiol-containing peptides. Specifically, a 4-arm PEG-norbornene monomer was reacted with cysteine-containing peptides to form a functional biomaterial network. This strategy has recently been demonstrated as a highly versatile platform for creating cytocompatible extracellular matrix (ECM) mimics.[22] Based on this strategy, we formed a hydrogel network using a broad range MMP-degradable crosslinker[27,28] and the common fibronectin-derived adhesion sequence RGDS[29,30] to provide

cells with a 3-dimensional environment permissive towards cell migration. A thiol-ene hydrogel formed using this strategy is predicted to have a mesh size that is much smaller than the size of a cell (13 ± 1 nm, see ESI,† calculating mesh size[31,32]), thereby limiting migration to proteolytic mechanisms. This polymerization scheme provides a versatile method for studying specific ECM properties while reducing confounding interactions caused by changes in materials properties or biological interactions that may be prevalent in more complex natural biomaterials. Fig. 1b–e demonstrates that thiol-ene hydrogels prepared using MMP-degradable crosslinkers and RGDS for adhesion are permissive towards cell proliferation and migration (see also Supplemental Movie 1†), similar to results recently reported for valvular interstitial cells.[26]

Previous migration studies have demonstrated that intermediate receptor densities promote maximum cell migration (*i.e.*, migration exhibits a "biphasic" dependence on receptor density) due to a balance of adhesive forces related to leading edge attachment and trailing edge detachment for both 2-dimensional and 3-dimensional culture platforms.[33–37] For this work, HT-1080s did not migrate in control gels containing non-biologically active RDGS (0 μM RGDS) or a non-degradable crosslinker (SH-PEG-SH instead of the MMP-degradable peptide), indicating that both adhesion and degradation are necessary for migration. The dependence of migration on degradation of the matrix confirms that the mesh size of the thiol-ene hydrogel as prepared here (13 ± 1 nm, see ESI,† calculating mesh size[31,32]) is too small for HT-1080s to migrate *via* a squeezing amoeboid mechanism. However, the results in Fig. 2 demonstrate that the introduction of RGDS combined with an MMP-degradable crosslinker promotes cell migration for all concentrations studied. The percentage of migrating HT-1080s (Fig. 2a) is particularly sensitive to RGDS concentration below 250 μM and reaches a maximum at 1000 μM. However, average distance to origin (total displacement from the initial starting position, Fig. 2b) and cell speed (Fig. 2c) were only weakly RGDS dependent while persistence (a measure of how long a cell migrates before changing direction) exhibited little or no RGDS dependence (Fig. 2d).

To further investigate the details of migration in thiol-ene hydrogels, we compared HT-1080s to dermal fibroblasts, a well-established mesenchymal cell type, with the results presented in Fig. 3. Fibroblasts in thiol-ene hydrogels exhibited a spread morphology with multiple protrusions (Fig. 3b, see also Supplemental Movie 2†) and migrated in a random fashion that resulted in cells being only moderately displaced from their initial position. While some HT-1080s also migrated with a spread morphology similar to fibroblasts, the predominant morphology was more rounded and generally exhibited only a single leading edge protrusion (Fig. 3a, see also Supplemental Movies 3 and 4†). Migration of rounded HT-1080s was usually in the direction of the leading edge protrusion and resulted in the cells following very long, relatively persistent paths through the synthetic matrix.

The difference in migration between HT-1080s and fibroblasts can be quantitatively demonstrated in several ways. In order to quantify the difference in morphology between
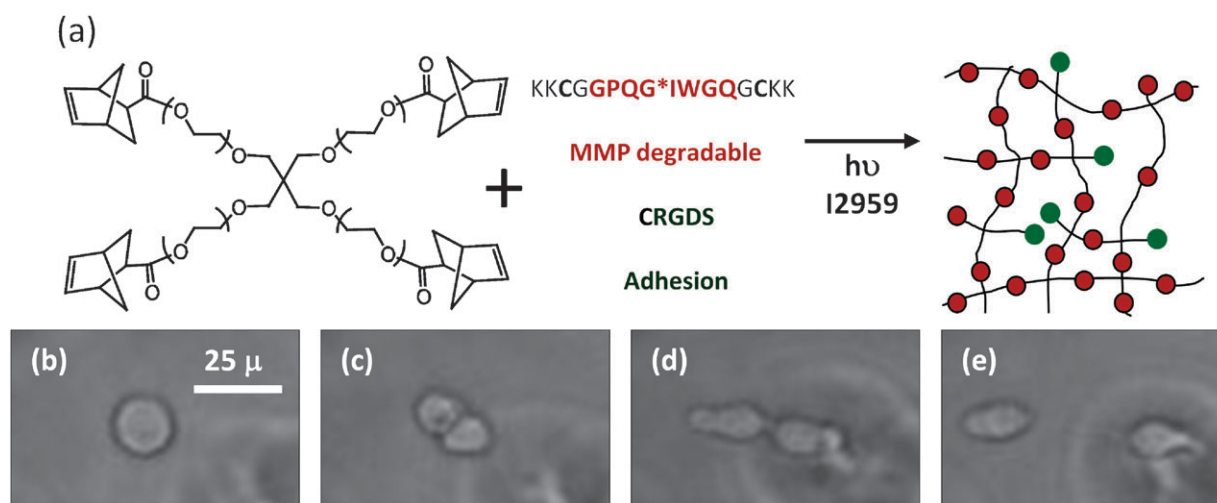
Fig. 1 Schematic representation of thiol-ene polymerization and example of cell division within the hydrogel formulation used here. (a) 20 000 M.W. 4-arm poly(ethylene glycol)-norbornene molecules were crosslinked with matrix metalloproteinase (MMP)-degradable peptides. A pendant CRGDS peptide was added at various concentrations to determine the effect of adhesion on cell proliferation and migration. To maintain constant materials properties, the total pendant peptide concentration was kept constant at 1500 μM by balancing CRGDS with the biologically inactive scrambled sequence CRDGS. All experiments were performed using hydrogels synthesized from 3% (by wt) monomer solutions. The thiol-ene scheme allows incorporation of any thiol-containing molecule and could therefore be used to study a number of cell–ECM interactions. (b–e) An example of how thiol-ene hydrogels are permissive towards important biological processes. Time lapse images of a dividing cell (See also Supplemental Movie 1†) and subsequent migration of daughter cells. HT-1080s were encapsulated in a thiol-ene hydrogel with 1000 μM CRGDS.

HT-1080s and fibroblasts, the elongation index (defined as the ratio of the cell long axis to the short axis) was calculated in hydrogels containing 1000 μM RGDS, with results presented in Table 1. The elongation index for fibroblasts was 3.0 ± 0.10 compared to 2.0 ± 0.04 for HT-1080s. The percentage of elongated cells (elongation index > 3) was also much greater for fibroblasts (36%) than for HT-1080s (10%) and there were fewer rounded cells (elongation index < 2, 37% for fibroblasts, 63% for HT-1080s). Further analysis (Fig. 3c) reveals that while there was only a moderate difference in speed between the two cell types, enhanced HT-1080 invasion was evident based on a much greater average distance to origin and persistence compared to fibroblasts (Fig. 3c). It was also determined that while >80% of HT-1080s migrate more than one cell length away from their initial position (>75% more than two cell lengths), <60% of fibroblasts migrate more than one cell length (<10% more than two cell lengths). Thus, these results illustrate that migration behavior is very different between these two mesenchymal cell types; while fibroblasts are only minimally migratory, HT-1080s are highly invasive in thiol-ene hydrogels.

The observation of a migration mode that was predominantly rounded was particularly interesting in light of recent work in which HT-1080s were shown to migrate through an amoeboid mechanism when proteolysis was blocked.[12,15] Previous work demonstrated that cancer cells migrating through a rounded morphology were dependent on the RhoA pathway,[13,15] and particularly its effector Rho-kinase (ROCK),[13] whereas cells utilizing a spread migration mode were RhoA (and ROCK[13]) independent.[13,15] Fig. 4 illustrates that ROCK inhibition had a very different effect on HT-1080s than on fibroblasts. While almost all fibroblasts adopted a highly spread morphology upon ROCK inhibition (Fig. 4b, Table 1)

(elongation index = 9.4 ± 0.50, 96% elongated, 2% rounded), a high percentage of HT-1080s remained rounded (Fig. 4d, Table 1) (elongation index 4.2 ± 0.30, 49% elongated, 41% rounded), with all rounded cells ceasing to migrate during the 6 h time scale of the experiment. Another characteristic of amoeboid migration is the formation of a constriction ring, a cell structure that is observed when amoeboid migrating cells squeeze through spaces that are smaller than the cell body.[12,38] Fig. 4e–h demonstrates that HT-1080s also appear to form constriction rings (indicated by arrow) in thiol-ene hydrogels (see also Supplemental Movie 5†). Thus, while proteolysis is strictly required for cells to migrate in the thiol-ene hydrogels used for this work, HT-1080 migration utilizes a mechanism with a high degree of amoeboid character.

Discussion

For the work reported here, we were interested in investigating the adhesion dependence of migration for mesenchymal cells that were limited to proteolytic modes of motility. We developed a synthetic ECM mimic in order to control specific components of the 3D extracellular environment and thus address the challenge of more precisely determining the influence of ECM on cell migration, in this case by quantitatively incorporating RGDS to study adhesion dependence. To our surprise, our results indicate that HT-1080 fibrosarcoma cells migrate in thiol-ene hydrogels through a mechanism that is not purely mesenchymal, but rather has many characteristics of amoeboid migration, even in the absence of external stimuli such as protease inhibitors or integrin blocking antibodies. Previous research has demonstrated that cancer cells (including HT-1080s) have the capacity to migrate through both
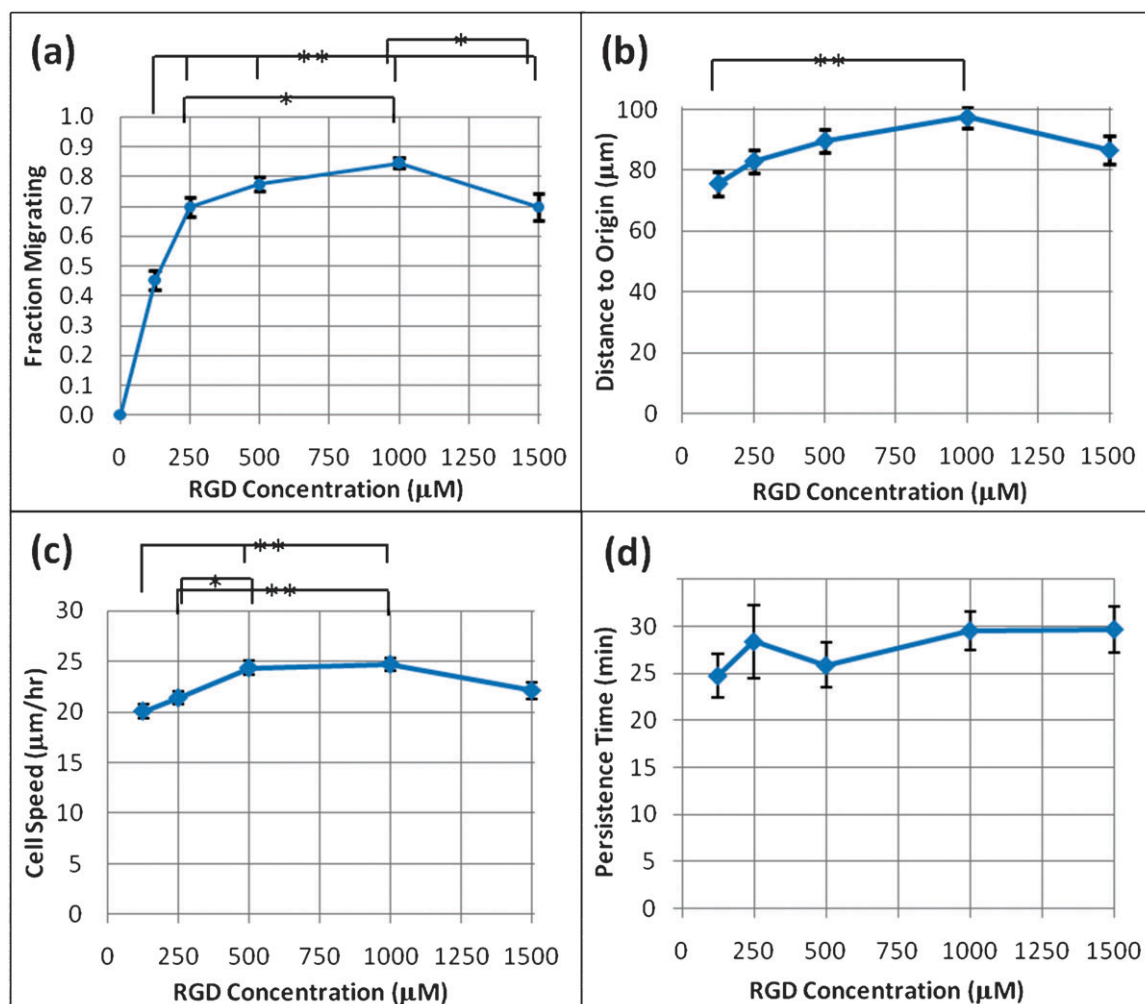
Fig. 2 The effect of RGDS concentration on migration. A migrating cell was defined as a cell that moved more than one cell length from its starting position (average cell length = 29 μm for HT-1080s). There were no migrating cells at 0 μM RGDS and thus a data point was not included for migration parameters at that concentration. (a) The average fraction of migrating cells in each field of view *vs.* RGDS concentration. (b) Average distance to origin at the end of 6 h *vs.* RGDS concentration. (c) Cell speed *vs.* RGDS concentration. (d) Persistence *vs.* RGDS concentration. Error bars for (a) represent standard error relative to total number of gels. Error bars for (b, c) represent standard error relative to individual cells ($N > 100$ for all concentrations). Error bars for (d) represent ± 95% confidence interval for the fit to the random walk equation (see Experimental section). All experiments were performed for 6 h with data collected in 15 min increments. Experiments were performed in triplicate with 3 separate gels per experiment (9 total gels, except 1500 μM RGDS in which $N = 8$). Statistical significance for (a–c) was determined with a one-way ANOVA followed by Tukey pairwise comparisons, $a = 0.05$ (*) or $a = 0.01$ (**). An estimate of significance for (d) can be found in Supplemental Fig. 2.†

mesenchymal and amoeboid mechanisms,[10–15] but transition to an amoeboid mode in at least some cases is dependent on collagen preparation.[12,16,17] Furthermore, cancer cells migrating *in vivo* appeared morphologically similar to rounded cells *in vitro*,[12,17] suggesting a more rounded mode of motility in a physiological environment than in naturally derived collagen. Thus, differences in the extracellular environment can profoundly influence migration mechanisms, and our results may indicate that cancer cells have the capacity to utilize aspects of both mesenchymal and amoeboid modes of migration.

Mesenchymal migration can be described by a basic progression that includes process extension, attachment, focalized proteolysis, contractility, and release.[5,10] A balance of adhesive forces leads to optimal mesenchymal migration at intermediate receptor density, termed "biphasic" or "bimodal" dependence.[21,33–37] In the thiol-ene hydrogels used for this work, HT-1080s did not migrate when the MMP-degradable peptide sequence (see Fig. 1) was replaced with a non-degradable poly(ethylene glycol) crosslinker, confirming that proteolysis is required in our system due to a very small mesh size (see ESI,† calculating mesh size). While migration in thiol-ene hydrogels required RGDS (cells do not migrate in 0 μM RGDS, Fig. 2a), HT-1080s exhibited only moderate biphasic RGDS dependence for speed and none for persistence, with significant invasive character being observed at even the lowest RGDS concentration studied (Fig. 2). Blocking β1 or β3 integrins for HT-1080s seeded in thiol-ene hydrogels had only a small effect on migration (see Supplemental Fig. 1†),
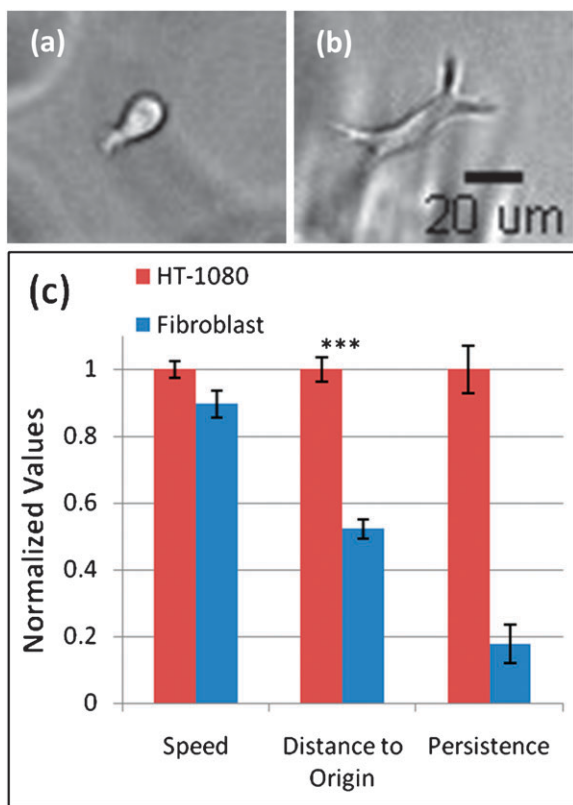
Fig. 3 Comparison of migration for HT-1080s and dermal fibroblasts in 1000 μM RGDS thiol-ene hydrogels. (a,b) Example of observed morphologies for (a) HT-1080s and (b) dermal fibroblasts. (a) While there were several morphologies observed for HT-1080s, most were rounded with a dynamic leading edge protrusion that defined the direction of migration (see also Supplemental Movies 3 and 4†) (b) Almost all fibroblasts adopted a typical spread, mesenchymal morphology (see also Supplemental Movie 2†). (c) Comparison of relative migration between HT-1080s and fibroblasts. Each parameter is normalized to HT-1080 values. Experiments were performed in triplicate with 3 separate gels per experiment (9 total gels). Error bars for speed and distance to origin represent standard error relative to individual cells ($N > 100$ for all experiments). Statistical significance was tested using a two-tailed Studen's t-test (***, $P < 0.00001$). Error bars for persistence represent ±95% confidence interval for the fit to the random walk equation (see Experimental section). See Supplemental Fig. 2† for persistence fits with confidence and prediction bands.

confirming that integrin dependence is weak. Unlike mesenchymal migration, amoeboid migrating cells glide through a porous network very rapidly *via* a squeezing and flowing mechanism with weak integrin dependence,[39–42] much like what is observed for adhesion dependence of HT-1080s in thiol-ene hydrogels. Additionally, constriction rings, which have been described for neutrophils[38] and HT-1080s migrating through an amoeboid mechanism[12] in natural biomaterials, were also observed for HT-1080s as they migrated through the 3-dimensional thiol-ene matrix (Fig. 4e–h, Supplemental Movie 5†). Thus, our results indicate that HT-1080s migrating in thiol-ene hydrogels exhibit at least some characteristics that would be expected for amoeboid migrating cells rather than mesenchymal cells.

A comparison to a well-established mesenchymal cell type, dermal fibroblasts, further indicates that HT-1080 migration in a thiol-ene hydrogel is not classically mesenchymal. While fibroblasts were spread (Fig. 3b and 4a, Supplemental Movie 2,† Table 1) with multiple protrusions, similar to what would be expected for a mesenchymal cell type, most HT-1080s were rounded with a single leading edge protrusion (Fig. 3a and Fig. 4c, Supplemental Movies 3 and 4,† Table 1). In order to quantify the degree of spreading, we calculated the elongation index (the ratio of the cell long axis to the short axis) for HT-1080s and fibroblasts (Table 1). In gels with 125 μM RGDS, most HT-1080s were rounded (88%, defined as an elongation index < 2.0) while almost none were elongated (1%, defined as an elongation index > 3.0), demonstrating that significant migration occurs even when a mesenchymal morphology is not observed. Increasing the RGDS concentration to 1000 μM led to a slight increase in elongated HT-1080s (10%) and a significant increase in elongation index (from 1.4 ± 0.03 to 2.0 ± 0.04), but the majority of the cells remained rounded (63%), indicating that while some cells may behave in a mesenchymal fashion, most do not. Blocking β1 or β3 integrins for HT-1080s seeded in thiol-ene hydrogels had only a small effect on morphology (Table 1), further emphasizing that integrin dependence was weak for HT-1080s migrating in thiol-ene hydrogels.

Fibroblasts were more spread than HT-1080s (elongation index of 3.0 ± 0.1 for fibroblasts compared to 2.0 ± 0.04 for HT-1080s, Table 1), with more elongated (36% *vs.* 10%) and fewer rounded (37% *vs.* 63%) cells. Blocking β1-integrin had a much larger influence on morphology for fibroblasts than for HT-1080s, with a large decrease in elongated cells (36 to 11%) corresponding to an increase in rounded cells (37 to 61%), as well as a large decrease in elongation index (3.0 ± 0.1 to 2.0 ± 0.07). The influence of integrin blocking on fibroblasts suggests that mesenchymal cells have the capacity to interact with thiol-ene hydrogels through integrin receptor interactions, and that HT-1080 migration and morphology are weakly dependent on adhesion due to a fundamental difference in mechanism rather than lack of appropriate receptors in the hydrogel. Thus, while there appears to be a subpopulation of HT-1080s in which spreading is influenced by adhesion similar to fibroblasts, most retain a morphology similar to amoeboid cells and behave very differently than the model mesenchymal cell type.

Of particular interest regarding the potential of our synthetic system for modeling cancer behavior, the elongation index for HT-1080s migrating in thiol-ene hydrogels (2.0 ± 0.04, Table 1) is similar to amoeboid migrating HT-1080s in collagen,[12] while the fraction of elongated cells (10% in thiol-ene) was much lower (>40% in collagen[15]). The HT-1080 strain used here adopted an elongated morphology in collagen, as well, indicating that the observed difference is not strain specific (see Supplemental Movie 6†). More importantly, the elongation index for HT-1080s in thiol-ene hydrogels was similar to that observed *in vivo* (based on reported elongation before proteolytic inhibition[12]). In contrast, the elongation index (3.0 ± 0.1) and fraction of elongated cells (36%) for fibroblasts are each very similar to spread HT-1080s in collagen,[12,15] suggesting that

Table 1 Comparison of cell elongation for cells encapsulated in thiol-ene hydrogels

HT-1080s	1000 RGD	*anti-β1*	ROCKi	125 RGD	*anti-β3*
Elongated	10%	9%	49%	1%	9%
Middle	28%	18%	11%	11%	19%
Rounded	63%	74%	41%	88%	72%
Elongation index	2.0 ± 0.04	1.8 ± 0.07	4.2 ± 0.30	1.4 ± 0.03	1.9 ± 0.10
P value (relative to HT-1080 1000 control)	—	<0.05	<0.00001	<0.00001	Not significant
Fibroblasts	**1000 RGD**	***anti-β1***	**ROCKi**		
Elongated	36%	11%	96%		
Middle	27%	28%	2%		
Rounded	37%	61%	2%		
Elongation Index	3.0 ± 0.10	2.00 ± 0.07	9.4 ± 0.50		
P value (relative to Fib 1000 control)	—	<0.00001	<0.00001		
P value (relative to HT-1080)	<0.00001	—	<0.00001		

Elongation index represents the ratio of the cell long axis to the short axis. Elongated cells are defined as having an elongation index > 3. Rounded cells are defined as having an elongation index < 2. For HT-1080s, each experiment included 1000 μM CRGDS (1000 RGD) along with indicated treatments (*anti-β1* or -β3, treated with β1 or β3 antibodies; ROCKi, treated with Rho-kinase inhibitor Y27632) except 125 RGD (125 μM CRGDS). For statistical analysis, each condition was compared to the 1000 μM CRGDS control (either HT-1080s or fibroblasts, 1000 RGD). Fibroblast data was also collected in 1000 μM CRGDS hydrogels plus indicated treatments. In addition to comparing *anti-β1* and ROCKi treated fibroblasts to control (1000 RGD), fibroblast control (Fib 1000) and ROCKi cells were compared to HT-1080 control (HT-1080 1000) and ROCKi cells. Elongation indices are reported as average±standard error and represent average cell values with N > 120 for all conditions. *P* values were calculated using a two-tailed Student's t-test. Rounding error leads to total cell counts of more than 100% for some conditions.

mesenchymal cells have the capacity to adopt normal morphologies when encapsulated in thiol-ene hydrogels and that there is a fundamental interaction that influences the metastatic, but not the healthy cell type. Specifically, the predominant migration mode for HT-1080s in thiol-ene hydrogels has a rounded morphology that closely matches *in vivo* migrating cells and *in vitro* amoeboid cells,[12] but is very different from spread mesenchymal cells (fibroblasts here, and HT-1080s in collagen[12,15]).

Researchers have previously demonstrated that rounded migrating cancer cells are sensitive to inhibition of the RhoA pathway, and particularly its effector[43] Rho-kinase (ROCK).[13] Thus, we investigated if HT-1080s migrating in thiol-ene hydrogels through a rounded morphology were similarly susceptible to inhibition of ROCK. ROCK-inhibition affected HT-1080s very differently compared to fibroblasts. While 96% of fibroblasts adopted an elongated morphology upon ROCK-inhibition, with only 2% remaining rounded (Fig. 4b, Table 1), only 49% of HT-1080s exhibited a similar elongated morphology. In contrast, 41% of HT-1080s remained rounded upon ROCK-inhibition (Fig. 4d, Table 1), and rounded cells ceased to migrate. The elongation was also much greater for fibroblasts (9.4 ± 0.50) than for HT-1080s (4.2 ± 0.30). Interestingly, the percentage of cells that remained rounded upon ROCK inhibition was similar to the percentage of migrating cells in 125 μM RGDS hydrogels, and may therefore indicate the true population of HT-1080s that behave in a unique fashion that is distinct from mesenchymal migration, with this subpopulation being RGDS independent but ROCK dependent. The loss of motility of rounded HT-1080s in thiol-ene hydrogels is in contrast to 2-dimensional experiments in which ROCK-inhibition did not block migration of A375m2 cells[13] and resulted in increased migration speed and percentage of migrating HT-1080s.[44] Thus, the decreased motility induced by ROCK inhibition for HT-1080s in thiol-ene hydrogels is similar to what has been observed for amoeboid migrating

cells,[13] and may be specific to 3-dimensional environments,[13,44] which could have implications for the importance of studying cancer migration in 3D.

Rounded, ROCK-dependent morphologies have previously been associated with increased invasion potential,[45] and Rho-ROCK signaling plays a role in a number of processes important for migration.[13–15,44–49] In 3D culture, the mesenchymal–amoeboid transition of HT-1080s resulted in decreased adhesion that was restored when RhoA-ROCK signaling was inhibited.[14] 2-Dimensional studies have demonstrated that RhoA-ROCK signaling negatively regulated integrin activity[44,49] and promoted migration of monocytes by limiting membrane protrusions and integrin activity to the leading edge.[50] Interestingly, the 2-dimensional HT-1080 morphology observed for this study was similar to monocytes[50] and very different than fibroblasts (Supplemental Movies 7 and 8†). Furthermore, time-resolved microscopy revealed that most HT-1080s migrated through long, highly directional paths in which the leading edge protrusion defined the direction of migration (Supplemental Movies 3 and 4†), similar to monocytes in 2D.[50] In contrast, fibroblasts displayed multiple protrusions, migrated in a seemingly random path, and for the most part were not displaced very far from their starting position (Supplemental Movie 2†). Quantitatively, cell speed was moderately enhanced for HT-1080s compared to fibroblasts (Fig. 3c). However, HT-1080s migrated in a much more persistent manner and invaded further than fibroblasts (Fig. 3c), demonstrating the enhanced invasion potential of the metastatic cell type. Therefore, our results indicate that HT-1080s are much more invasive than fibroblasts and that invasiveness is ROCK dependent. We speculate that the observed rounded morphology and the leading edge protrusion each play an important role in the highly invasive nature of HT-1080s and that RhoA-ROCK may be crucial for maintaining this phenotype or controlling cell mechanics essential for cell movement.
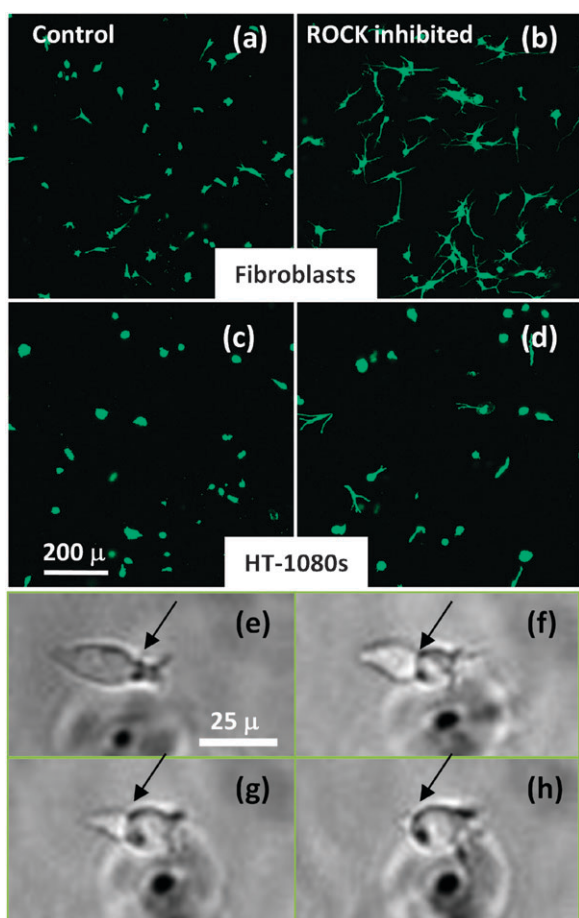
Fig. 4 The effects of Rho-kinase (ROCK)-inhibition for HT-1080 fibrosarcoma cells and dermal fibroblasts. Morphologies for (a) fibroblast control, (b) ROCK-inhibited fibroblasts, (c) HT-1080 control and (d) ROCK-inhibited HT-1080s. Upon ROCK inhibition, most fibroblasts adopt a highly spread morphology (b). Similar spread morphologies are observed for HT-1080s, but a high fraction of cells remain rounded (d). (e)–(h) Time series demonstrates that a migrating HT-1080 forms an apparent constriction ring (indicated by arrow), a type of cellular structure that has been observed for amoeboid migrating cells (See also Supplemental Movie 5†). Each frame represents a 15 min increment.

Taken together, the results presented here indicate that a sub-population of HT-1080 fibrosarcoma cells migrate through a mechanism that is distinct from the mesenchymal mode previously described.[12] HT-1080s migrating in thiol-ene hydrogels are morphologically similar to what has been observed in vivo[12] and closely resemble an amoeboid migration mode in vitro,[12,15] but are very different than mesenchymal cells both in 2D[50] and 3D[12] (as well as fibroblasts in this work). Furthermore, the invasive sub-population of HT-1080s migrating in thiol-ene hydrogels are only weakly RGDS dependent and highly susceptible to ROCK-inhibition, which are both characteristics of amoeboid migrating cells.[13–15,39–42,49,50] HT-1080s have the capacity to adapt to different stimuli by switching between mesenchymal and amoeboid migration,[12,15] indicating that at least some cells can utilize the machinery of both mechanisms. Thus, the observed migration mode for HT-1080s in thiol-ene hydrogels,

and possibly in vivo as well, may not be truly amoeboid or mesenchymal but rather a hybrid mechanism with characteristics of both. Further investigation will be required to characterize the observed migration mode for HT-1080s in thiol-ene hydrogels, to understand the factors that induce this behavior, and to determine the physiological relevance of our results. However, the observation of a previously unreported migration mechanism that quantitatively captures aspects of in vivo observations[12] is exciting and demonstrates that an engineering strategy combined with current biological methods could broaden our understanding of cancer progression and metastasis.

Care must be taken when interpreting results in simple materials such as synthetic hydrogels since they lack many of the biological characteristics present in the in vivo environment. However, some ECM characteristics may be better captured by a synthetic hydrogel than naturally derived biomaterials, including stiffness, porosity that prevents non-proteolytic migration mechanisms, and the incorporation of ligands that access a wide range of integrins (collagen only contains $\beta 1$-integrin receptors[51] while RGDS is a receptor for a many integrins[52]), and these differences may help to explain our results here. Also, the use of a synthetic approach allows ECM character to be systematically incorporated into thiol-ene hydrogels, and thus researchers can tailor the 3-dimensional environment to the specific question they are trying to answer. While the material design for this study incorporates only simple functional characteristics of the ECM, more complex strategies can be envisioned in which combinations of thiol-containing biomolecules are covalently bound to the thiol-ene backbone or intact biomolecules such as proteins are sequestered within the 3-dimensional matrix. Thus, we hope that this work demonstrates the utility of a synthetic approach as a promising new tool that will complement current biological methods and allow questions to be explored that would have otherwise been impossible using naturally derived biomaterials.

Experimental

Synthesis of 4-arm poly(ethylene glycol)-norbornene[22]

All reagents were purchased from Sigma-Aldrich unless otherwise noted. All scales are molar equivalents relative to hydroxyls on 4-arm poly(ethylene glycol) (PEG). PEG norbornene was prepared by the addition of norbornene acid via symmetric anhydride DCC coupling. While stirring, 3 × N,N'-dicyclohexylcarbodiimide (DCC) and 6 × 5-norbornene-2-carboxylic acid (norbornene acid may need to be melted if solid at RT) was added to a round bottom flask. Then, dichloromethane (DCM, absolute, >99.5%, Fluka) was transferred to the flask containing DCC and norbornene acid using inert atmosphere conditions and positive pressure transfer. Shortly after addition of the acid, a white byproduct precipitate was observed (dicyclohexylurea) indicating the formation of dinorbornene anhydride. Reagents were blanketed in argon while stirring and allowed to react at room temperature for 30 min.

In a separate reaction vessel, 4-arm PEG (MW 20 000, JenKemUSA, Allen, TX) was dissolved in DCM (absolute, >99.5%, Fluka) with 5 × pyridine and 0.5 × 4-(dimethyl-amino)pyridine (DMAP). After the anhydride solution (first flask) was allowed to stir for 30 min, the PEG solution (second flask) was added using a syringe. The reaction was blanketed again with argon and stirred overnight at room temperature. The reaction mixture was then filtered with a glass fritted Buchner funnel (medium frit), the filtrate was washed with 5% sodium bicarbonate solution and the product was precipitated from the organic phase in ice cold diethyl ether. The precipitate was filtered and then dried under vacuum. Proton NMR was used to characterize substitution and purity of the product. If purity was <95%, washing steps were repeated.

Peptide synthesis

All peptides were synthesized on solid Rink-amide resin using Fmoc chemistry on an Applied Biosystems 433A peptide synthesizer at the 0.25 mmol scale. Lysines were added to the terminal positions of the peptide sequences to increase solubility and glycines adjacent to the active sequence were used as spacers. Peptides were cleaved from resin and deprotected in trifluoroacetic acid (TFA) with 10% deionized water, 5% phenol, 5% dithiothreitol (DTT, Research Products International) and 2% triisopropylsilane (TIPS) while stirring in the dark for 4 h. Peptides were then precipitated in 0 °C diethyl ether and centrifuged/washed 5× with 0 °C diethyl ether. After the fifth wash with diethyl ether, the pellet was resuspended in deionized water, frozen, and lyophilized to yield a fluffy, white peptide cake. As peptides prepared by this method often contain substantial amounts of bound water, the true peptide content was determined by using the absorbance of the peptide solution at 280 nm with a molar extinction coefficient for tryptophan of 5500 M^{-1} cm^{-1}. To verify the absorbance results and to verify the presence and content of reduced thiols, an Ellman's assay (Pierce) was performed using freshly prepared L-cysteine solutions to generate a standard curve. Finally, each peptide was analyzed by reverse phase HPLC and MALDI mass spectrometry to confirm that purity of the peptide was ≥ 95%.

Cell culture

HT-1080s were obtained from ATCC and cultured in Alpha MEM (Lonza) supplemented with 10% Fetal Bovine Serum (Gibco), 1% Pen. Strep. (Gibco), and 0.2% fungizone (Gibco). All experiments were performed with HT-1080s passaged between P6 and P8. Primary neonatal human fibroblasts (NHF) were kindly provided by Professor R. Rivkah Isseroff, Department of Dermatology, University of California-Davis and cultured in Dubellco's Modified Eagle's Medium (DMEM, Gibco) supplemented with 10% FBS, 1% Pen. Strep., and 0.2% fungizone. Experiments with fibroblasts were performed with cells between P6 and P9.

Encapsulating cells

Cells were trypsinized and the suspension was mixed well and counted with a hemacytometer. For experiments in which receptor density dependence was measured, 1.5 mL of a 3% by weight solution of PEG-norbornene/MMP-degradable peptide crosslinker mixture was prepared. 100 μL of the monomer was added to each of 5 vials. 15 μL total volume of 25 mM RGDS and 25 mM RDGS solutions were added to the 100 μL monomer solutions, mixed in the proper ratios to give the reported RGDS concentrations, with total concentration equal to 1500 μM RGDS + RDGS for all solutions (uncorrected for volume peptide added). 300 000 cells were pelleted using a centrifuge and resuspended in the 1.0 mL remaining monomer solution. Then, 150 μL cell/monomer suspension was added to each vial and mixed thoroughly by pipetting. 30 μL aliquots were then added to the cut end of a 1 mL syringe tip and polymerized under ∼10 mW cm^{-2}, 352 nm centered UV light (XX series UVP lamp) for 3 min. The polymerized hydrogels were then suspended in appropriate media and allowed to swell overnight. For all other experiments, a similar procedure was followed, but monomer solutions were prepared as needed in 250 μL aliquots. For non-degradable control, the MMP-degradable cross-linker was replaced with SH-PEG-SH (MW = 3400, Laysan Bio Inc.).

Real-time migration experiments

Hydrogels were prepared as described above. After hydrogels were allowed to swell overnight, they were placed in the bottom of 24-well culture insert plates (BD Falcon, Fisher), immobilized with culture inserts (BD Falcon, Fisher) in which a 5 mm biopsy punch was used to create a hole in the center, and suspended in 1.5 mL fresh media. Hydrogels were ∼1 mm thick after swelling. Cells were monitored in real time to determine migration parameters using a Nikon TE2000-E microscope with fully automated control of stage position and image collection, controlled with Metamorph software, and a Nikon environmental chamber with external heater (In vivo Scientific) and CO_2 regulator (In vivo Scientific) to control heat and CO_2 levels. In order to ensure that no surface cells were included in the migration analysis, z-stacks of only the middle 500 μm of the gels were imaged. After being placed on the microscope, gels were equilibrated for 2 h to allow the plate to reach the desired temperature and CO_2 levels. Images were then collected every 15 min for 6 h.

Rho-kinase (ROCK) inhibition experiments

Cells were seeded in MMP-degradable hydrogels with 1000 μM RGD as described above and exposed to 10 μM Y27632 for 2 h prior to placing samples on the microscope. For morphology images, cells were incubated in 2 mM calcein (Invitrogen) for 30 min and images were collected using a Zeiss Axioplan 2 confocal microscope. 3-Dimensional z-stacked images were flattened to 2D for display. The percentage of migrating cells for ROCK inhibition studies was not determined since only very spread cells migrated upon ROCK inhibition, and distinguishing the cell body from extending processes was impossible for most cells. No rounded cells were observed to migrate in the 6 h time course of the real time experiments.

Image analysis

z-stacks of migrating cells were flattened to 2D images and cells were tracked using Metamorph software. Cells that interacted, divided, or did not migrate a minimum of one cell length during the 6 h time course were not included in migration calculations. One cell length was defined as the average long axis length of a cell (29 μM for HT-1080s or 39 μM for fibroblasts). The distance migrated was determined for the position at all time points during the 6 h experiment, and thus cells that migrated more than one cell length at any time point were included even if the final distance was less than the minimum length. For average distance to origin (reported in Fig. 3 and 4), only the distance at the final time point was used.

Persistence calculations

A sliding window algorithm[53] was used to calculate mean squared displacements (*MSD*) at various time intervals (*t*). Persistence calculations were performed by fitting mean-squared displacement data to a persistent random walk model with speed being unrestricted (calculated speeds were slightly higher than experimentally determined speeds). The random walk equation used was:

$$MSD = 2S^2 P[t - P(1 - e^{-\frac{t}{p}})]$$

where *S* is cell speed, *P* is directional persistence time, and *t* is the total time. The error for each data point was calculated by IGOR software (Wavemetrics) as the square root of the diagonal elements of the covariance matrix and reported as a ±95% confidence interval. Examples of fitting are provided in Supplemental Fig. 2.†

Acknowledgements

References

1 M. J. Bissell, H. G. Hall and G. Parry, *J. Theor. Biol.*, 1982, **99**, 31–68.
2 C. M. Nelson and M. J. Bissell, *Annu. Rev. Cell Dev. Biol.*, 2006, **22**, 287–309.
3 J. T. Erler and V. M. Weaver, *Clin. Exp. Metastasis*, 2009, **26**, 35–49.
4 M. J. Bissell and D. Radisky, *Nat. Rev. Cancer*, 2001, **1**, 46–54.
5 D. A. Lauffenburger and A. F. Horwitz, *Cell*, 1996, **84**, 359–369.
6 L. G. Griffith and M. A. Swartz, *Nat. Rev. Mol. Cell Biol.*, 2006, **7**, 211–224.
7 E. Cukierman, R. Pankov, D. R. Stevens and K. M. Yamada, *Science*, 2001, **294**, 1708–1712.
8 E. Cukierman, R. Pankov and K. M. Yamada, *Curr. Opin. Cell Biol.*, 2002, **14**, 633–639.
9 K. B. Hotary, E. D. Allen, P. C. Brooks, N. S. Datta, M. W. Long and S. J. Weiss, *Cell*, 2003, **114**, 33–45.
10 P. Friedl and K. Wolf, *Nat. Rev. Cancer*, 2003, **3**, 362–374.
11 Y. Hegerfeldt, M. Tusch, E. B. Brocker and P. Friedl, *Cancer Res.*, 2002, **62**, 2125–2130.
12 K. Wolf, I. Mazo, H. Leung, K. Engelke, U. H. von Andrian, E. I. Deryugina, A. Y. Strongin, E. B. Brocker and P. Friedl, *J. Cell Biol.*, 2003, **160**, 267–277.
13 E. Sahai and C. J. Marshall, *Nat. Cell Biol.*, 2003, **5**, 711–719.
14 N. O. Carragher, S. M. Walker, L. S. A. Carragher, F. Harris, T. K. Sawyer, V. G. Brunton, B. W. Ozanne and M. C. Frame, *Oncogene*, 2006, **25**, 5726–5740.
15 D. Yamazaki, S. Kurisu and T. Takenawa, *Oncogene*, 2009, **28**, 1570–1583.
16 F. Sabeh, I. Ota, K. Holmbeck, H. Birkedal-Hansen, P. Soloway, M. Balbin, C. Lopez-Otin, S. Shapiro, M. Inada, S. Krane, E. Allen, D. Chung and S. J. Weiss, *J. Cell Biol.*, 2004, **167**, 769–781.
17 F. Sabeh, R. Shimizu-Hirota and S. J. Weiss, *J. Cell Biol.*, 2009, **185**, 11–19.
18 M. P. Lutolf and J. A. Hubbell, *Nat. Biotechnol.*, 2005, **23**, 47–55.
19 M. P. Lutolf, *Integr. Biol.*, 2009, **1**, 235–241.
20 J. L. West and J. A. Hubbell, *Macromolecules*, 1999, **32**, 241–244.
21 M. P. Lutolf, J. L. Lauer-Fields, H. G. Schmoekel, A. T. Metters, F. E. Weber, G. B. Fields and J. A. Hubbell, *Proc. Natl. Acad. Sci. U. S. A.*, 2003, **100**, 5413–5418.
22 B. D. Fairbanks, M. P. Schwartz, A. E. Halevi, C. R. Nuttelman, C. N. Bowman and K. S. Anseth, *Adv. Mater.*, DOI: 10.1002/adma.200901808.
23 G. P. Raeber, M. P. Lutolf and J. A. Hubbell, *Acta Biomater.*, 2007, **3**, 615–629.
24 G. P. Raeber, M. P. Lutolf and J. A. Hubbell, *Biophys. J.*, 2005, **89**, 1374–1388.
25 M. R. Lutolf, F. E. Weber, H. G. Schmoekel, J. C. Schense, T. Kohler, R. Muller and J. A. Hubbell, *Nat. Biotechnol.*, 2003, **21**, 513–518.
26 J. A. Benton, B. D. Fairbanks and K. S. Anseth, *Biomaterials*, 2009, **30**, 6593–6603.
27 S. Netzel-Arnett, G. B. Fields, H. Birkedal-Hansen, H. E. Van Wart and G. Fields, *J. Biol. Chem.*, 1991, **266**, 6747–6755.
28 H. Nagase and G. B. Fields, *Biopolymers*, 1996, **40**, 399–416.
29 E. Ruoslahti and M. D. Pierschbacher, *Science*, 1987, **238**, 491–497.
30 M. D. Pierschbacher and E. Ruoslahti, *Nature*, 1984, **309**, 30–33.
31 T. Canal and N. A. Peppas, *J. Biomed. Mater. Res.*, 1989, **23**, 1183–1193.
32 K. S. Anseth, C. N. Bowman and L. BrannonPeppas, *Biomaterials*, 1996, **17**, 1647–1657.
33 S. P. Palecek, J. C. Loftus, M. H. Ginsberg, D. A. Lauffenburger and A. F. Horwitz, *Nature*, 1997, **385**, 537–540.
34 P. A. Dimilla, J. A. Stone, J. A. Quinn, S. M. Albelda and D. A. Lauffenburger, *J. Cell Biol.*, 1993, **122**, 729–737.
35 B. T. Burgess, J. L. Myles and R. B. Dickinson, *Ann. Biomed. Eng.*, 2000, **28**, 110–118.
36 M. H. Zaman, L. M. Trapani, A. Siemeski, D. MacKellar, H. Y. Gong, R. D. Kamm, A. Wells, D. A. Lauffenburger and P. Matsudaira, *Proc. Natl. Acad. Sci. U. S. A.*, 2006, **103**, 10889–10894.
37 M. H. Zaman, P. Matsudaira and D. A. Lauffenburger, *Ann. Biomed. Eng.*, 2007, **35**, 91–100.
38 J. T. H. Mandeville, M. A. Lawson and F. R. Maxfield, *J. Leukocyte Biol.*, 1997, **61**, 188–200.
39 P. Friedl, S. Borgmann and E. B. Brocker, *J. Leukocyte Biol.*, 2001, **70**, 491–509.
40 A. F. Brown, *J. Cell Sci.*, 1982, **58**, 455–467.
41 W. S. Haston, J. M. Shields and P. C. Wilkinson, *J. Cell Biol.*, 1982, **92**, 747–752.
42 T. Lämmermann, B. L. Bader, S. J. Monkley, T. Worbs, R. Wedlich-Soldner, K. Hirsch, M. Keller, R. Förster, D. R. Critchley, R. Fässler and M. Sixt, *Nature*, 2008, **453**, 51–55.
43 I. Ishizaki, M. Maekawa, K. Fujisawa, K. Okawa, A. Iwamatsu, A. Fujita, N. Watanabe, Y. Saito, A. Kakizuka, N. Morii and S. Narumiya, *EMBO J.*, 1996, **15**, 1885–1893.
44 V. Niggli, M. Schmid and A. Nievergelt, *Biochem. Biophys. Res. Commun.*, 2006, **343**, 602–608.
45 K. Itoh, K. Yoshioka, H. Akedo, M. Uehata, T. Ishizaki and S. Narumiya, *Nat. Med.*, 1999, **5**, 221–225.
46 K. Amano, K. Chihara, K. Kimura, Y. Fukata, N. Nakamura, Y. Matsuura and K. Kaibuchi, *Science*, 1997, **275**, 1308–1311.
47 K. Kimura, M. Ito, M. Amano, K. Chihara, Y. Fukata, M. Nakafuku, B. Yamamori, J. H. Feng, T. Nakano, K. Okawa, A. Iwamatsu and K. Kaibuchi, *Science*, 1996, **273**, 245–248.
48 J. Alblas, L. Ulfman, P. Hordijk and L. Koenderman, *Mol. Biol. Cell*, 2001, **12**, 2137–2145.
49 R. A. Worthylake, S. Lemoine, J. M. Watson and K. Burridge, *J. Cell Biol.*, 2001, **154**, 147–160.
50 R. A. Worthylake and K. Burridge, *J. Biol. Chem.*, 2003, **278**, 13578–13584.
51 D. J. White, S. Puranen, M. S. Johnson and J. Heino, *Int. J. Biochem. Cell Biol.*, 2004, **36**, 1405–1410.
52 E. Ruoslahti, *Annu. Rev. Cell Dev. Biol.*, 1996, **12**, 697–715.
53 R. B. Dickinson and R. T. Tranquillo, *AIChE J.*, 1993, **39**, 1995–2010.